Pharmacological Research 172 (2021) 105850

Contents lists available at ScienceDirect

Pharmacological Research

journal homepage: www.elsevier.com/locate/yphrs

ABCB1 and ABCG2, but not CYP3A4 limit oral availability and brain accumulation of the RET inhibitor pralsetinib

Yaogeng Wang [a], Rolf W. Sparidans [b], Sander Potters [c], Maria C. Lebre [a], Jos H. Beijnen [a,b,d], Alfred H. Schinkel [a,*]

[a] The Netherlands Cancer Institute, Division of Pharmacology, Plesmanlaan 121, 1066 CX Amsterdam, The Netherlands
[b] Utrecht University, Faculty of Science, Department of Pharmaceutical Sciences, Division of Pharmacology, Universiteitsweg 99, 3584 CG Utrecht, The Netherlands
[c] Leiden university, Faculty of Science, Leiden Academic Centre for Drug Research (LACDR), Einsteinweg 55, 2300 RA Leiden, The Netherlands
[d] The Netherlands Cancer Institute, Department of Pharmacy & Pharmacology, Plesmanlaan 121, 1066 CX Amsterdam, The Netherlands

ARTICLE INFO

Keywords:
Pralsetinib
Cytochrome P450-3A
Oral availability
P-glycoprotein/ABCB1
BCRP/ABCG2
Brain accumulation

Chemical compounds:
Cabozantinib (PubChem CID: 25102847)
Elacridar (PubChem CID: 119373)
Pralsetinib (PubChem CID: 129073603)
Selpercatinib (PubChem CID: 134436906)
Vandetanib (PubChem CID: 3081361)
Zosuquidar (PubChem CID: 3036703)

ABSTRACT

Background and purpose: Pralsetinib is an FDA-approved oral small-molecule inhibitor for treatment of rearranged during transfection (RET) proto-oncogene fusion-positive non-small cell lung cancer. We investigated how the efflux transporters ABCB1 and ABCG2, the SLCO1A/1B uptake transporters and the drug-metabolizing enzyme CYP3A influence pralsetinib pharmacokinetics.

Experimental approach: In vitro, transepithelial pralsetinib transport was assessed. *In vivo*, pralsetinib (10 mg/kg) was administered orally to relevant genetically modified mouse models. Pralsetinib concentrations in cell medium, plasma samples and organ homogenates were measured using liquid chromatography-tandem mass spectrometry.

Key results: Pralsetinib was efficiently transported by human (h)ABCB1 and mouse (m)Abcg2, but not hACBG2. *In vivo*, mAbcb1a/1b markedly and mAbcg2 slightly limited pralsetinib brain penetration (6.3-and 1.8-fold, respectively). Testis distribution showed similar results. *Abcb1a/1b;Abcg2*$^{-/-}$ mice showed 1.5-fold higher plasma exposure, 23-fold increased brain penetration, and 4-fold reduced recovery of pralsetinib in the small intestinal content. mSlco1a/1b deficiency did not affect pralsetinib oral availability or tissue exposure. Oral coadministration of the ABCB1/ABCG2 inhibitor elacridar boosted pralsetinib plasma exposure (1.3-fold) and brain penetration (19.6-fold) in wild-type mice. Additionally, pralsetinib was a modest substrate of mCYP3A, but not of hCYP3A4, which did not noticeably restrict the oral availability or tissue distribution of pralsetinib.

Conclusions and implications: SLCO1A/1B and CYP3A4 are unlikely to affect the pharmacokinetics of pralsetinib, but ABCG2 and especially ABCB1 markedly limit its brain and testis penetration, as well as oral availability. These effects are mostly reversed by oral coadministration of the ABCB1/ABCG2 inhibitor elacridar. These insights may be useful in the further clinical development of pralsetinib.

1. Introduction

The rearranged during transfection (RET) proto-oncogene encodes a receptor tyrosine kinase for members of the glial cell line-derived neurotrophic factor (GDNF) family of extracellular signaling molecules [1, 2]. RET is a single-pass transmembrane protein with a typical intracellular tyrosine kinase domain and is involved in many different physiological and developmental functions. When mutated, loss of RET causes the absence of enteric ganglia from the distal colon (Hirschsprung's disease) and congenital megacolon, demonstrating an important role of RET in the development of the enteric nervous system [3]. RET mutations occur in most medullary thyroid cancers (MTCs) [4],

Abbreviations: ABC, ATP-binding cassette; ABCB1, ATP-binding cassette sub-family B member 1; ABCG2, ATP-binding cassette sub-family G member 2; BBB, blood-brain-barrier; BCRP, breast cancer resistance protein; BTB, blood-testis-barrier; CYP, Cytochrome P450; Cyp3aXAV, Cyp3a knockout mice with specific expression of human CYP3A4 in liver and intestine; h as prefix, human; LC-MS/MS, liquid chromatography coupled with tandem mass spectrometry; MDCK, Madin-Darby canine kidney; m as prefix, mouse; MKIs, Multikinase inhibitors; OATP, Organic-anion-transporting polypeptide; P-gp, P-glycoprotein; RET, Rearranged during transfection (RET) proto-oncogene; SLCO, organic anion solute carrier family; TKI, tyrosine kinase inhibitor.

* Corresponding author.
E-mail address: a.schinkel@nki.nl (A.H. Schinkel).

https://doi.org/10.1016/j.phrs.2021.105850
Received 19 June 2021; Received in revised form 2 August 2021; Accepted 21 August 2021
Available online 25 August 2021

whereas RET fusions occur in various types of cancer, including 1–2% of lung cancers, up to 10–20% of papillary thyroid cancers, and albeit rarely, in many other solid tumors [5]. Besides, RET alterations have also been uncovered at low frequency by next generation sequencing (NGS) of large numbers of patient tumors in other tumor types, including ovarian epithelial carcinoma and salivary gland adenocarcinoma [6].

Although some multikinase inhibitors (MKIs) with nonselective RET inhibitory activity have been available to treat RET-altered cancers, patients have derived only modest benefit from these so far, with unexpected side-effects [7]. For example, cabozantinib was used for RET-mutant MTCs [8] and RET fusion-positive lung cancers [9] and vandetanib for advanced or metastatic medullary thyroid cancer [10] and advanced non-small-cell lung cancer [11]. However in 2020, the FDA approved two highly selective, ATP-competitive small-molecule RET inhibitors, selpercatinib (LOXO-292, RETEVMO, Eli Lilly) [12] and pralsetinib (Blu-667, GAVRETO, Roche) [13]. Both can be applied for the treatment of adults with metastatic RET-fusion positive non-small cell lung cancer (NSCLC), yielding higher objective response rates (ORRs) of 68% and 58%, respectively, compared to other multikinase inhibitors, such as cabozantinib therapy with an ORR of only 28% [14,15]. According to the guidelines, the recommended dose in adults is 160 mg twice daily for selpercatinib [12] and 400 mg once daily for pralsetinib [13]. Besides, they were designed to have high bioavailability and significant central nervous system (CNS) penetration, which may induce more efficient therapy for brain metastasis occurring in NSCLC patients. However, compared to selpercatinib, the information on pralsetinib pharmacokinetic properties is still limited.

Drug absorption, distribution, metabolism and excretion (ADME) can be influenced by certain efflux and influx transporters such as the ATP-binding cassette (ABC) transporters and the organic anion transporting polypeptides (OATPs). They can thus influence the pharmacokinetics, and hence the safety and efficacy profiles of specific drugs [16–18]. Considering the high expression of the ABC drug efflux transporters P-glycoprotein (P-gp; ABCB1) and breast cancer resistance protein (BCRP; ABCG2) at the apical membrane of enterocytes, hepatocytes and renal tubular epithelial cells, they could potentially limit intestinal absorption of their substrates or mediate their direct intestinal, hepatobiliary or renal excretion. Moreover, ABCB1 and ABCG2 are also highly expressed in brain capillary endothelial cells of the blood-brain barrier (BBB), where their efflux capacity can protect the central nervous system (CNS) from exogenous toxic compounds [19]. Conversely, limited exposure of the brain to anticancer drugs because of these transporters may reduce their therapeutic efficacy, especially against brain metastases [20–23]. In addition, ABC transporters are also expressed in many tumor types, potentially mediating multidrug resistance against anticancer drugs [19]. As pralsetinib targets different tumor types with RET fusions that may develop brain metastases (especially lung cancer), it is important to know whether pralsetinib is transported by ABCB1 and/or ABCG2 *in vivo*, potentially affecting its oral availability and brain accumulation.

Organic anion-transporting polypeptides (OATPs), encoded by SLCO genes, are sodium-independent transmembrane uptake transporters for endogenous and exogenous compounds like hormones, toxins, and numerous drugs [24]. The SLCO1A/1B proteins are of particular interest because of their broad substrate specificities and their high expression in the liver where they may affect oral availability and liver disposition of certain drugs [25–29]. Thus, we wanted to know whether pralsetinib is a substrate of SLCO1A/1B and whether this can influence pralsetinib oral availability and organ distribution.

Besides these transporters, the multidrug-metabolizing Cytochrome P450 3A (CYP3A) enzyme complex is responsible for most Phase I drug metabolism. CYP3A4 is the most abundant CYP enzyme in human liver, and involved in the metabolism of about 50% of the currently used drugs, resulting in drug inactivation or sometimes also activation [30–32]. CYP3A enzymes have high variation in activity between, but also within individuals due to drug–drug interactions and genetic polymorphisms. This can cause oral availability and plasma exposure differences among patients, which may dramatically influence their therapeutic efficacy and toxicity.

The primary aim of this study was to clarify the *in vivo* roles of ABCB1, ABCG2 and SLCO1A/1B (OATP1A/1B) as well as CYP3A in modulating oral availability and/or brain accumulation of pralsetinib by transepithelial pralsetinib transport assay *in vitro* and using appropriate genetically modified mouse models. We also studied the effect of co-administration of the ABCB1 and ABCG2 inhibitor elacridar on pralsetinib overall exposure and tissue distribution.

2. Materials and methods

2.1. Cell lines and transport assays

Polarized dog kidney-derived Madin-Darby Canine Kidney (MDCK-II) cells and their stably transduced subclones expressing human (h) ABCB1, hABCG2, or mouse (m) Abcg2 cDNA were used and cultured as described [33,34]. Transepithelial transport assays were performed on microporous polycarbonate membrane filters (3.0 μm pore size, 12 mm diameter, Transwell 3414). Parental and variant subclones were seeded at a density of 2.5×10^5 cells per well and cultured for 3 days to form an intact monolayer. Membrane tightness was assessed by measurement of transepithelial electrical resistance (TEER) using an Epithelial Volt-Ohm Meter (Merck Millipore, Darmstadt, Germany) before and after the transport phase.

For inhibition experiments, 5 μM zosuquidar (ABCB1 inhibitor) and/or 5 μM Ko143 (ABCG2/Abcg2 inhibitor) were used during the transport experiments. Cells were pre-incubated with one or a combination of the inhibitors for 1 h in both apical and basolateral compartments. The transport phase was started (t = 0) by replacing the medium in either the apical or the basolateral compartment with fresh DMEM including 10% (v/v) fetal bovine serum (FBS) and pralsetinib at 5 μM, as well as the appropriate inhibitor(s). Plates then were kept at 37 °C in 5% (v/v) CO_2 during the experiment, and 50 μl aliquots were taken from the acceptor compartment at 1, 2, 4, and 8 h, and stored at −30 °C until LC-MS/MS measurement of the pralsetinib concentrations. Experiments were performed in triplicate and the mean transport is shown in the figure. Active transport was expressed using the transport ratio r, *i.e.*, the amount of apically directed drug transport divided by basolaterally directed drug translocation after 8 h (h).

2.2. Animals

Mice were housed and handled according to institutional guidelines complying with Dutch and EU legislation. All experimental animal protocols were evaluated and approved by the institutional animal care and use committee. Wild-type (both female and male), *Abcb1a/1b*$^{-/-}$ (male), *Abcg2*$^{-/-}$ (male), *Abcb1a/1b;Abcg2*$^{-/-}$ (male), *Slco1a/1b*$^{-/-}$ (male), *Cyp3a*$^{-/-}$ (female) and *Cyp3aXAV* (female) mice, all of a > 99% FVB genetic background, were used between 9 and 16 weeks of age. Animals were kept in a temperature-controlled environment with 12-h light and 12-h dark cycle and they received a standard diet (Transbreed, SDS Diets, Technilab – BMI) and acidified water *ad libitum*.

2.3. Drug solutions

For oral administration, pralsetinib was dissolved in dimethyl sulfoxide (DMSO) at a concentration of 50 mg/ml and further diluted with polysorbate 20, 100% ethanol and 5% glucose water, resulting in a final working solution of 1 mg/ml in [DMSO: Polysorbate 20: 100% ethanol: 5% glucose water = 2: 15: 15: 68, (v/v/v/v)]. Elacridar hydrochloride was dissolved in DMSO (53 mg/ml) in order to get 50 mg elacridar base per ml DMSO. The stock solution was further diluted with a mixture of polysorbate 20, 100% ethanol and 5% glucose water to yield an

elacridar concentration of 5 mg/ml in [DMSO: Polysorbate 20: 100% ethanol: 5% glucose water = 10: 15: 15: 60, (v/v/v/v)]. All dosing solutions were prepared freshly on the day of the experiment.

2.4. Plasma and organ pharmacokinetics of pralsetinib in mice

In order to minimize variation in absorption because of oral administration, mice were first fasted for 3 h before pralsetinib (10 mg/kg) was administered orally, using a blunt-ended needle. For the 4 h transporter pilot experiments, tail vein blood samples were collected at 0.125, 0.25, 0.5, 1, and 2 h time points after oral administration, respectively. For the 2 h transporter main experiments and elacridar inhibition experiments, tail vein blood samples were collected at 0.125, 0.25, 0.5, and 1 h time points after oral administration, respectively. For the 8 h CYP3A experiments, tail vein blood sampling was performed at 0.25, 0.5, 1, 2, and 4 h, respectively. Blood sample (~50 μl) collection was performed using microvettes containing dipotassium-EDTA. At the last time point in each experiment (2, 4, or 8 h), mice were anesthetized with 5% isoflurane and blood was collected by cardiac puncture in Eppendorf tubes containing heparin as an anticoagulant. The mice were then sacrificed by cervical dislocation and brain, liver, kidney, lung, small intestine (SI), small intestine contents (SIC) and testis were rapidly removed. Plasma was isolated from the blood by centrifugation at 9000 g for 6 min at 4 °C, and the plasma fraction was collected and stored at −30 °C until analysis. Organs were homogenized with 4% (w/v) bovine serum albumin and stored at −30 °C until analysis. The relative tissue-to-plasma ratio after oral administration was calculated by determining the pralsetinib tissue concentration relative to the pralsetinib plasma concentration at the last time point.

2.5. LC-MS/MS analysis

Pralsetinib concentrations in DMEM/FBS (9/1, v/v) (Invitrogen, Waltham, MA, USA) cell culture medium, plasma samples, and organ homogenates were determined using a validated liquid chromatography-tandem mass spectrometry assay as described [35].

2.6. Materials

Pralsetinib was purchased from MedChemExpress (Monmouth Junction, NJ, USA). Zosuquidar and elacridar HCl were obtained from Sequoia Research Products (Pangbourne, UK). Ko143 was from Tocris Bioscience (Bristol, UK). Bovine Serum Albumin (BSA) Fraction V was obtained from Roche Diagnostics GmbH (Mannheim, Germany). Glucose water 5% w/v was from B. Braun Medical Supplies (Melsungen, Germany). Isoflurane was purchased from Pharmachemie (Haarlem, The Netherlands), heparin (5000 IU ml^{-1}) was from Leo Pharma (Breda, The Netherlands). All other chemicals used in the pralsetinib detection assay were described before [35]. All other chemicals and reagents were obtained from Sigma-Aldrich (Steinheim, Germany).

2.7. Data and statistical analysis

Pharmacokinetic parameters were calculated by non-compartmental methods using the PK solver software [36]. The area under the plasma concentration-time curve (AUC) was calculated using the trapezoidal rule, without extrapolating to infinity. The peak plasma concentration (C_{max}) and the time of maximum plasma concentration (T_{max}) were estimated from the original (individual mouse) data. One-way analysis of variance (ANOVA) was used when multiple groups were compared and the Bonferroni *post hoc* correction was used to accommodate multiple testing. The two-sided unpaired Student's *t*-test was used when treatments or differences between two specific groups were compared using the software GraphPad Prism7 (GraphPad Software, La Jolla, CA, USA). All the data were log-transformed before statistical tests were applied. Differences were considered statistically significant when $P < 0.05$. All data are presented as mean ± SD.

3. Results

3.1. In vitro transport of pralsetinib

Transepithelial drug transport was tested by using polarized monolayers of Madin-Darby Canine Kidney (MDCK-II) parental cells and various ABC transporter-overexpressing derivative cell lines. No significant transport of pralsetinib (5 μM) by the low-level endogenous canine Abcb1 present in the parental MDCK-II cells [37] was observed either without or with ABCB1 inhibitor zosuquidar (r = 1.2, Fig. 1A and r = 1.2, Fig. 1B). In cells overexpressing hABCB1, there was strong apically directed transport of pralsetinib (r = 19, Fig. 1C), which could be completely inhibited by zosuquidar (r = 1.0, Fig. 1D).

Zosuquidar was added to inhibit any possible contribution of endogenous canine Abcb1 in subsequent experiments with MDCK-II cells overexpressing hABCG2 and mAbcg2. The ABCG2 inhibitor Ko143 was used to inhibit the transport activity of hABCG2 and mAbcg2. In hABCG2-overexpressing MDCK-II cells, there was no detectable apically directed transport of pralsetinib in the absence or presence of Ko143 (r = 1.0, Fig. 1E; r = 0.9, Fig. 1F). We also observed marked apically directed transport of pralsetinib in cells overexpressing mouse Abcg2 (r = 7.1) and this was virtually abrogated by Ko143 (r = 1.0, Fig. 1G and H).

Pralsetinib thus appears to be efficiently transported by hABCB1 and mAbcg2, but not by hABCG2 and canine ABCB1 *in vitro*.

3.2. Impact of ABCB1, ABCG2 and SLCO1A/1B on pralsetinib plasma pharmacokinetics and tissue disposition

Pralsetinib is orally administered in the clinic, so we performed a 4 h oral pharmacokinetic pilot study in male wild-type, *Abcb1a/1b;Abcg2*$^{-/-}$ and *Slco1a/1b*$^{-/-}$ mice using 10 mg/kg pralsetinib to study the possible impact of ABCB1A/1B, ABCG2 and OATP1A/1B on oral bioavailability and tissue disposition of pralsetinib. As shown in Supplemental Fig. 2 and Supplemental Table 1, even though *Abcb1a/1b;Abcg2*$^{-/-}$ mice had slightly higher plasma exposure of pralsetinib compared to wild-type mice, there was no statistically significant difference in AUC or C_{max} of pralsetinib between them. However, the last time point (4 h) in *Abcb1a/1b;Abcg2*$^{-/-}$ mice did show a significantly higher plasma concentration, suggesting a somewhat delayed pralsetinib elimination in this strain. It took around two hours to reach the maximum plasma concentration of pralsetinib for these two mouse strains (average C_{max} in wild-type and *Abcb1a/1b;Abcg2*$^{-/-}$ mice are 6202 ng/ml and 6962 ng/ml, respectively), indicating that absorption of this compound is not very rapid as compared to many other TKI drugs in mice [38–41]. Notably, the T_{max} and C_{max} results obtained in our mouse models are of the same order of magnitude as those observed in patients (T_{max} ranging from 2 to 4 h with average C_{max} 2830 ng/ml).

Brain, liver, kidney, small intestine (SI), small intestine contents (SIC), testis, lung and spleen concentrations of pralsetinib 4 h after oral administration were also assessed. The pralsetinib brain-to-plasma ratio (0.022) in wild-type mice was very low, suggesting poor brain penetration of pralsetinib (Supplemental Table 1). The brain concentration and brain-to-plasma ratio in *Abcb1a/1b;Abcg2*$^{-/-}$ mice were increased by 44.9-fold and 32.3-fold, respectively, compared to those in wild-type mice (Supplemental Fig. 3 and Supplemental Table 1). *Slco1a/1b*$^{-/-}$ mice also showed somewhat enhanced brain concentrations and brain-to-plasma ratios by 1.7-fold and 1.5-fold, respectively. Likewise in testis, the testis-to-plasma ratio was low in wild-type mice (0.13), and combined Abcb1 and Abcg2 deficiency could increase the ratio to 0.71 (5.5-fold increase).

Tissue-to-plasma ratios in other organs were not meaningfully altered among the three strains (Supplemental Fig. 4 and Supplemental Fig. 5). However, for the small intestine content (SIC) matrix, we found

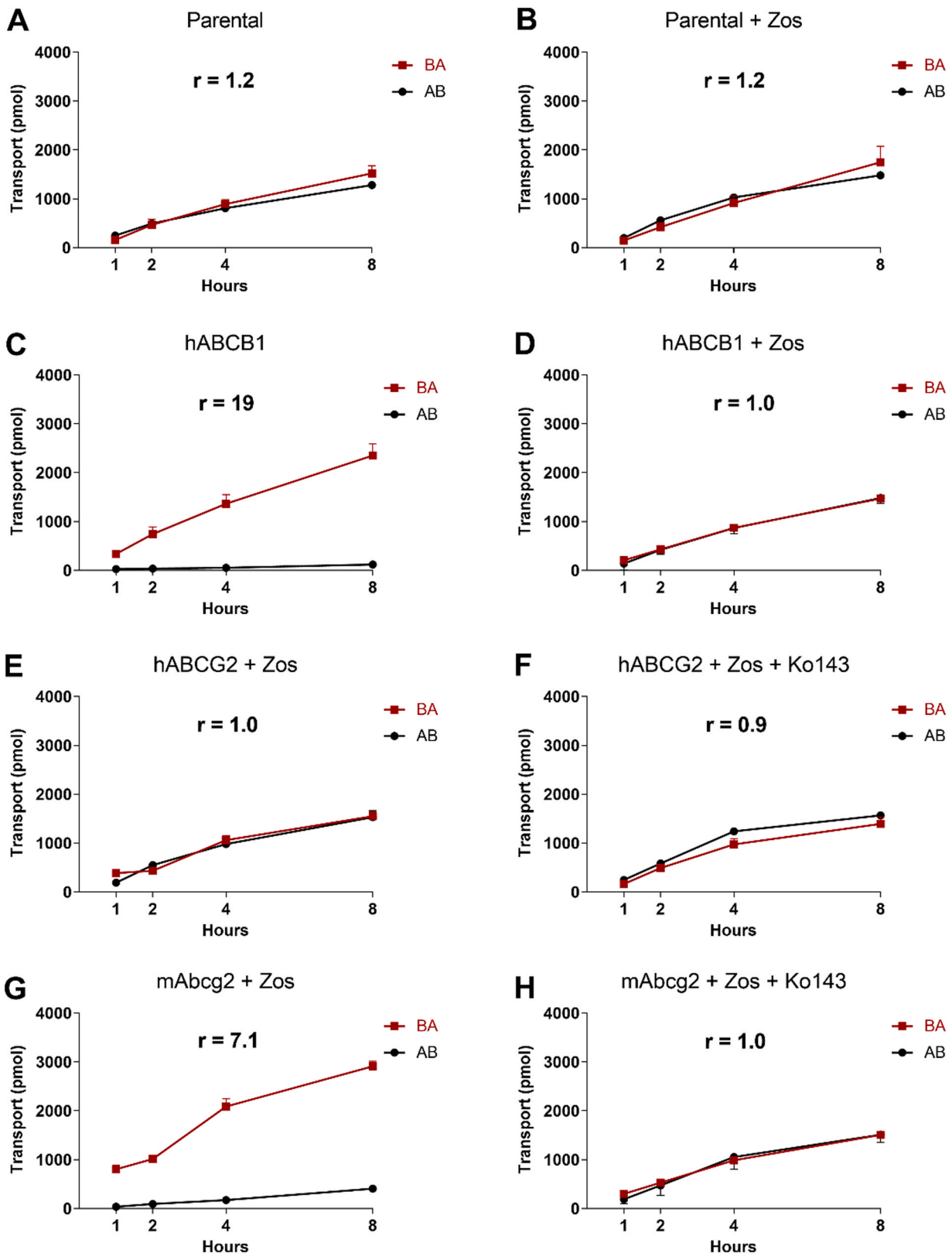

Fig. 1. Transepithelial transport of pralsetinib (5 μM) assessed in MDCK-II cells either non-transduced (A, B), transduced with hABCB1 (C, D), hABCG2 (E, F) or mAbcg2 (G, H) cDNA. At t = 0 h, drug was applied in the donor compartment and the concentrations in the acceptor compartment at t = 1, 2, 4 and 8 h were measured and plotted as pralsetinib transport (pmol) in the graph (n = 3). B, D, F, H: Zosuquidar (Zos, 5 μM) was applied to inhibit human and/or endogenous canine ABCB1. F and H: the ABCG2 inhibitor Ko143 (5 μM) was applied to inhibit ABCG2/Abcg2–mediated transport. *r*, relative transport ratio. AB (•), translocation from the apical to the basolateral compartment; BA (■),translocation from the basolateral to the apical compartment. Points, mean; bars, S.D.

that the percentage of dose recovered was markedly decreased in *Abcb1a/1b/Abcg2*$^{-/-}$ mice compared to wild-type mice (0.11, 9-fold Supplemental Fig. 5E and Supplemental Table 1). These results may indicate that pralsetinib was absorbed more rapidly across the gut wall or that there was reduced hepatobiliary excretion of the absorbed pralsetinib in the absence of both Abcb1a/1b and Abcg2.

In wild-type mice most tissue-to-plasma ratios for liver, kidney, and small intestine (all > 1) were far higher than those observed for the brain (0.022) and even testis (0.13), suggesting the strong impact of the blood-brain-barrier (BBB) and blood-testis-barrier (BTB) on reducing tissue accumulation of pralsetinib. We did not observe any sign of acute spontaneous toxicity of pralsetinib in any of the three mouse strains, even though there was a dramatic increase in pralsetinib brain accumulation in *Abcb1a/1b;Abcg2*$^{-/-}$ mice.

As shown in Supplemental Fig. 2 and Supplemental Table 1, the pralsetinib plasma $AUC_{0-4\,h}$, C_{max} and T_{max} were not significantly different between wild-type and *Slco1a/1b*$^{-/-}$ mice. With respect to tissues, even though the deficiency of mSlco1a/1b slightly increased brain-to-plasma ratio (from 0.022 to 0.034), lung-to-plasma ratio, and kidney-to-plasma ratio, and decreased liver-to-plasma ratio (from 3.4 to 2.7), the changes were limited. We also did not find any significant differences in pralsetinib percentage of dose recovered in SIC between wild-type and *Slco1a/1b*$^{-/-}$ mice (Supplemental Figs. 3–5). Taken together, these results indicate that pralsetinib pharmacokinetics is not substantially influenced by SLCO1A/1B activity.

3.3. ABCB1 and ABCG2 limit pralsetinib brain and testis exposure

The separate and combined functions of Abcb1a/1b and Abcg2 in modulating oral bioavailability and tissue distribution of pralsetinib were subsequently studied by administering pralsetinib (10 mg/kg) orally to wild-type, *Abcb1a/1b*$^{-/-}$, *Abcg2*$^{-/-}$, and *Abcb1a/1b/Abcg2*$^{-/-}$ mice. The experiment was terminated at 2 h, when pralsetinib plasma levels were still close to the C_{max}. As shown in Fig. 2 and Table 1, single deficiency of either mAbcb1 or mAbcg2 resulted in higher pralsetinib plasma exposure, with the plasma $AUC_{0-2\,h}$ increased in both *Abcb1a/1b*$^{-/-}$ (1.5-fold, $P < 0.01$) and *Abcg2*$^{-/-}$ (1.2-fold, albeit not statistically significant) mice (Table 1). Such increase also showed up in combination *Abcb1a/1b/Abcg2*$^{-/-}$ mice, 1.6-fold compared to wild-type mice ($P < 0.01$). Abcb1a/1b activity appeared to be the main factor limiting plasma exposure.

Pralsetinib brain concentrations in *Abcb1a/1b*$^{-/-}$ and *Abcb1a/1b/Abcg2*$^{-/-}$ mice were profoundly increased by 9.5-fold and 30.4-fold respectively, and only slightly increased by 1.8-fold in *Abcg2*$^{-/-}$ mice compared to wild-type mice. The brain-to-plasma ratio of pralsetinib was again very low (0.040) in wild-type mice, but could be increased to 0.25 (6.3-fold) due to single mAbcb1 deficiency and further up to 0.92 (23-fold) by combined mAbcb1 and mAbcg2 deficiency (Fig. 3A and B; Table 1). Again, this increase was limited in mAbcg2-deficient mice (0.072, 1.8-fold). These results reveal that Abcb1a/1b and Abcg2 can both restrict pralsetinib brain penetration, although Abcb1a/1b is the dominant player. In the absence of Abcb1a/1b activity, Abcg2 noticeably limits pralsetinib brain penetration (by about 3.7-fold), while when Abcg2 is absent, Abcb1a/1b could still take over almost the whole transport function. Qualitatively similar results were obtained for pralsetinib testis penetration, although the wild-type testis-to-plasma ratio was substantially higher (0.060), and the relative increases in ratios in *Abcb1a/1b*$^{-/-}$ (4.5-fold) and *Abcb1a/1b/Abcg2*$^{-/-}$ (7.8-fold) mice were more modest than observed for brain (Fig. 3C and D; Table 1). These data indicate that Abcb1a/1b and, to a lesser extent, Abcg2 can strongly reduce the brain accumulation of pralsetinib, while testis accumulation was more modestly affected.

With respect to other organs, we observed lower SI-to-plasma ratios in *Abcb1a/1b*$^{-/-}$ and *Abcb1a/1b/Abcg2*$^{-/-}$ mice (Supplemental Fig. 7B), which did not show up in *Abcg2*$^{-/-}$ mice. As small intestine often mainly reflects the small intestine contents concentrations, we also analyzed

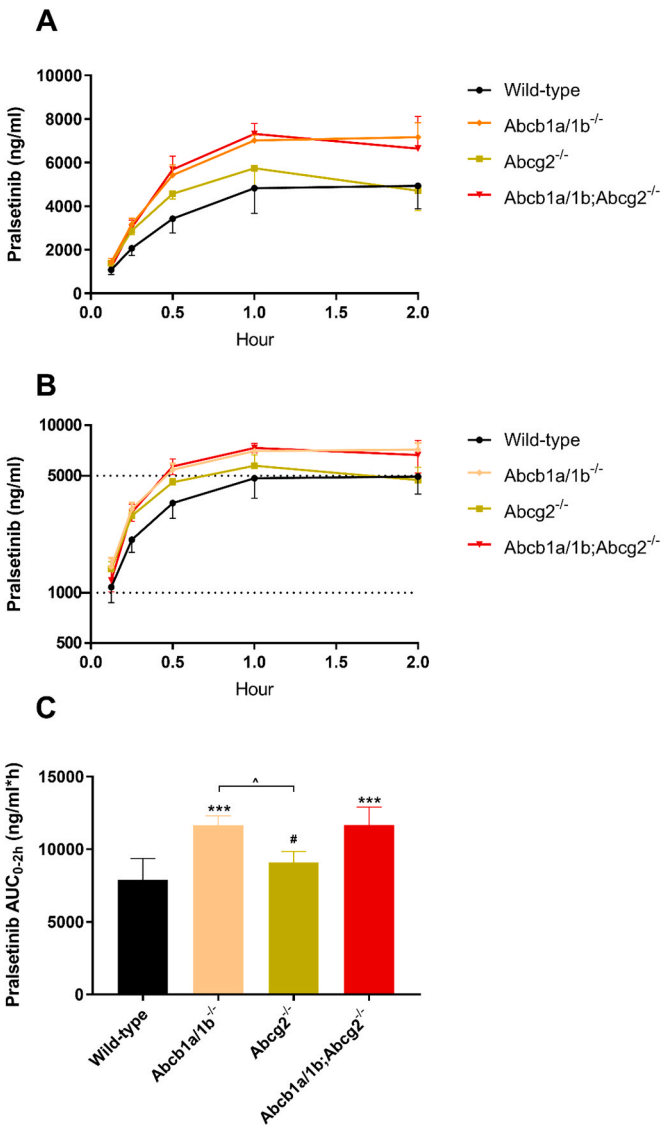

Fig. 2. Plasma concentration-time curves (A), semi-log plot of plasma concentration-time curves (B) and plasma $AUC_{0-2\,h}$ (C) of pralsetinib in male wild-type, *Abcb1a/1b*$^{-/-}$, *Abcg2*$^{-/-}$ and *Abcb1a/1b;Abcg2*$^{-/-}$ mice over 2 h after oral administration of 10 mg/kg pralsetinib. Data are given as mean ± S.D. (n = 6). * $P < 0.05$; ** $P < 0.01$; *** $P < 0.001$ compared to wild-type mice; # $P < 0.05$; ## $P < 0.01$; ### $P < 0.001$ compared to *Abcb1a/1b;Abcg2*$^{-/-}$ mice. Statistical analysis was applied after log-transformation of linear data.

related parameters of the SIC. Indeed, the SIC percentage of total dose values were markedly reduced from 12.0% to 3.2% in *Abcb1a/1b*$^{-/-}$ mice (0.27-fold) and to 2.9% in *Abcb1a/1b;Abcg2*$^{-/-}$ mice (0.24-fold) compared to wild-type mice, whereas this decrease was much less in *Abcg2*$^{-/-}$ mice (7.1%, 0.59-fold) (Supplemental Fig. 7 and Table 1). These findings were consistent with our pilot results. They may indicate a more rapid and extensive absorption of pralsetinib across the intestinal wall in the absence of intestinal Abcb1a/1b activity (essentially because of loss of an intestinal excretion process), or reduced hepatobiliary recirculation of absorbed pralsetinib through biliary excretion mediated by Abcb1a/1b in the bile canaliculi of the liver, or a combination of both processes. No meaningful differences were found in tissue-to-plasma ratios of other tissues (Supplemental Fig. 6).

Table 1
Plasma and organ pharmacokinetic parameters of pralsetinib in male wild-type, *Abcb1a/1b*$^{-/-}$, *Abcg2*$^{-/-}$ and *Abcb1a/1b*; *Abcg2-/-* mice over 2 h after oral administration of 10 mg/kg pralsetinib.

Parameter	Genotype			
	Wild-type	*Abcb1a/1b*$^{-/-}$	*Abcg2*$^{-/-}$	*Abcb1a/1b;Abcg2*$^{-/-}$
$AUC_{0-2\,h}$, ng/ml*h	7898 ± 1469	11,657 ± 643***	9094 ± 747#	11,663 ± 1248***
Fold change $AUC_{0-2\,h}$	1.0	1.5	1.2	1.5
C_{max}, ng/ml	5181 ± 1117	7301 ± 520**	5890 ± 833#	7510 ± 631***
T_{max}, h	1.5 ± 0.55	1.7 ± 0.52	1.3 ± 0.61	1.3 ± 0.52
C_{brain}, ng/g	186 ± 62	1774 ± 125***###	339 ± 107*###	5658 ± 2176***
Fold change C_{brain}	1.0	9.5	1.8	30.4
Brain-to-plasma ratio	0.040 ± 0.018	0.25 ± 0.017***###	0.072 ± 0.017###	0.92 ± 0.46***
Fold change ratio	1.0	6.3	1.8	23
C_{Liver}, ng/g	16,558 ± 1976	23,385 ± 3547**	18,702 ± 2187#	24,295 ± 3712***
Fold increase C_{liver}	1.0	1.4	1.1	1.5
Liver-to-plasma ratio	3.4 ± 0.47	3.3 ± 0.50	4.1 ± 1.3	3.8 ± 0.75
Fold change ratio	1.0	0.97	1.2	1.1
C_{SI}, ng/g	20,412 ± 2964	14,214 ± 2372	20,994 ± 5971	14,344 ± 4333
Fold change C_{SI}	1.0	0.70	1.0	0.70
SI-to-plasma ratio	4.3 ± 1.2	2.0 ± 0.23**	4.8 ± 2.3##	2.2 ± 0.70**
Fold change ratio	1.0	0.47	1.1	0.51
SIC percentage of dose, %	12.0 ± 3.8	3.2 ± 1.5***	7.1 ± 1.9##	2.9 ± 1.3***
Fold change ratio	1.0	0.27	0.59	0.24
C_{testis}, ng/g	287 ± 95	1910 ± 206***##	327 ± 23###	2997 ± 515***
Fold change C_{testis}	1.0	6.7	1.1	10.4
Testis-to-plasma ratio	0.060 ± 0.016	0.27 ± 0.044***##	0.071 ± 0.014###	0.47 ± 0.11***
Fold change ratio	1.0	4.5	1.2	7.8

Data are given as mean ± S.D. (n = 6). $AUC_{0-2\,h}$, area under the plasma concentration-time curve; C_{max}, maximum concentration in plasma; T_{max}, time point (h) of maximum plasma concentration; C_{brain}, brain concentration; C_{liver}, liver concentration; SI, small intestine (tissue); C_{SI}, small intestine tissue concentration; SIC, small intestine contents; C_{testis}, testis concentration; * $P < 0.05$; ** $P < 0.01$; *** $P < 0.001$ compared to wild-type mice; # $P < 0.05$; ## $P < 0.01$; ### $P < 0.001$ compared to *Abcb1a/1b;Abcg2*$^{-/-}$ mice. Statistical analysis was applied after log-transformation of linear data.

3.4. Effect of the dual ABCB1 and ABCG2 inhibitor elacridar on pralsetinib brain accumulation

As pralsetinib penetration into wild-type brain was markedly restricted by ABCB1 and ABCG2 activity, we investigated to what extent the dual ABCB1 and ABCG2 inhibitor elacridar could increase brain accumulation of pralsetinib, and whether it would influence pralsetinib disposition and distribution in other tissues. This approach may potentially be used for enhancing pralsetinib brain accumulation and therapeutic efficacy. Considering that the elacridar plasma exposure peak occurs approximately 4 h after oral administration in mice, elacridar (50 mg/kg) or vehicle was administered orally 2 h prior to oral pralsetinib administration (10 mg/kg) to wild-type and *Abcb1a/1b;Abcg2*$^{-/-}$ mice. Plasma and brain pralsetinib levels were assessed 2 h later, at which time point pralsetinib plasma concentrations were still high, making the impact of the BBB transporters especially relevant. When elacridar was absent, the pralsetinib plasma $AUC_{0-2\,h}$ was significantly (1.5-fold) increased in *Abcb1a/1b;Abcg2*$^{-/-}$ mice compared to wild-type mice, consistent with preceding experiments. Pre-treatment with elacridar increased plasma pralsetinib $AUC_{0-2\,h}$ by 1.3-fold in wild-type mice, and did not alter exposure in *Abcb1a/1b;Abcg2*$^{-/-}$ mice (Fig. 4 and Table 2).

With respect to tissues, in the absence of elacridar, the brain concentration and brain-to-plasma ratio of pralsetinib was 45.9-fold and 31.9-fold higher in *Abcb1a/1b;Abcg2*$^{-/-}$ than in wild-type mice, respectively ($P < 0.001$), (Fig. 5A and B and Table 2). Elacridar pre-treatment markedly increased these parameters in wild-type mice by 26.2- and 19.6-fold, respectively ($P < 0.001$), yielding a level similar to that in elacridar pre-treated *Abcb1a/1b;Abcg2*$^{-/-}$ mice (35.5- and 20.0-fold, respectively). While the data indicate extensive inhibition of Abcb1a/1b and Abcg2 activity in the BBB by elacridar, the brain penetration in both elacridar co-administration groups was somewhat (about 40%) lower than that in vehicle-treated *Abcb1a/1b;Abcg2*$^{-/-}$ mice. This suggested a modest additional effect of elacridar, somewhat lowering brain penetration of pralsetinib independent of the ABC transporters. Unlike for brain, for testis the enhanced pralsetinib penetration by elacridar only showed up in wild-type mice, suggesting full inhibition of ABC transporter functions in the BTB by elacridar (Fig. 5C and D and Table 2). Relative drug penetration in most other tissues (liver, kidney, lung and spleen) was not meaningfully altered by elacridar in wild-type or *Abcb1a/1b;Abcg2*$^{-/-}$ mice (Supplemental Fig. 8B, D, F and H).

In accordance with our previous results, there was a large amount of pralsetinib in the intestinal lumen at 2 h in wild-type mice, with 20.2% of dose recovered in SI+SIC. This was markedly reduced to 8.4% upon elacridar co-administration (Supplemental Fig. 9). Even though there was a small difference in recovered pralsetinib between *Abcb1a/1b;Abcg2*$^{-/-}$ mice with elacridar (11.7%) compared with *Abcb1a/1b;Abcg2*$^{-/-}$ mice without elacridar (7.5%), the results became virtually identical after correction for the plasma concentrations (Supplemental Fig. 9D). Taken together, these results suggest that the mouse Abcb1a/1b and Abcg2 in the small intestine and/or the bile canaliculi of the liver were completely inhibited by the elacridar treatment, resulting in decreased recovery of pralsetinib in the small intestine contents.

3.5. Impact of CYP3A on pralsetinib plasma pharmacokinetics and tissue disposition

To investigate the possible *in vivo* impact of mouse Cyp3a and human CYP3A4 on pralsetinib pharmacokinetics, we performed an 8 h study in female wild-type, *Cyp3a*$^{-/-}$ and Cyp3aXAV mice (*Cyp3a*$^{-/-}$ mice with transgenic expression of human CYP3A4 in liver and intestine). Pralsetinib (10 mg/kg) was administered orally after 2–3 h of fasting, blood samples were taken at several time points, and at 8 h organs were collected. The pralsetinib plasma $AUC_{0-8\,h}$ in *Cyp3a*$^{-/-}$ mice was significantly higher (1.4-fold, $P < 0.01$) than that in wild-type mice (Fig. 6 and Table 3). *Cyp3a*$^{-/-}$ mice had a similar T_{max} as wild-type mice (about 2 h), but the difference between the two mouse strains occurred mainly during the first 4 h. After that, the relative elimination was similar between the strains (Fig. 6B). These data suggest that mCyp3a modestly reduces pralsetinib exposure, presumably mainly by first-pass (intestinal?) metabolism. Intriguingly, for the Cyp3aXAV mice we observed a similar plasma profile as in *Cyp3a*$^{-/-}$ mice up till 2 h, but after that,

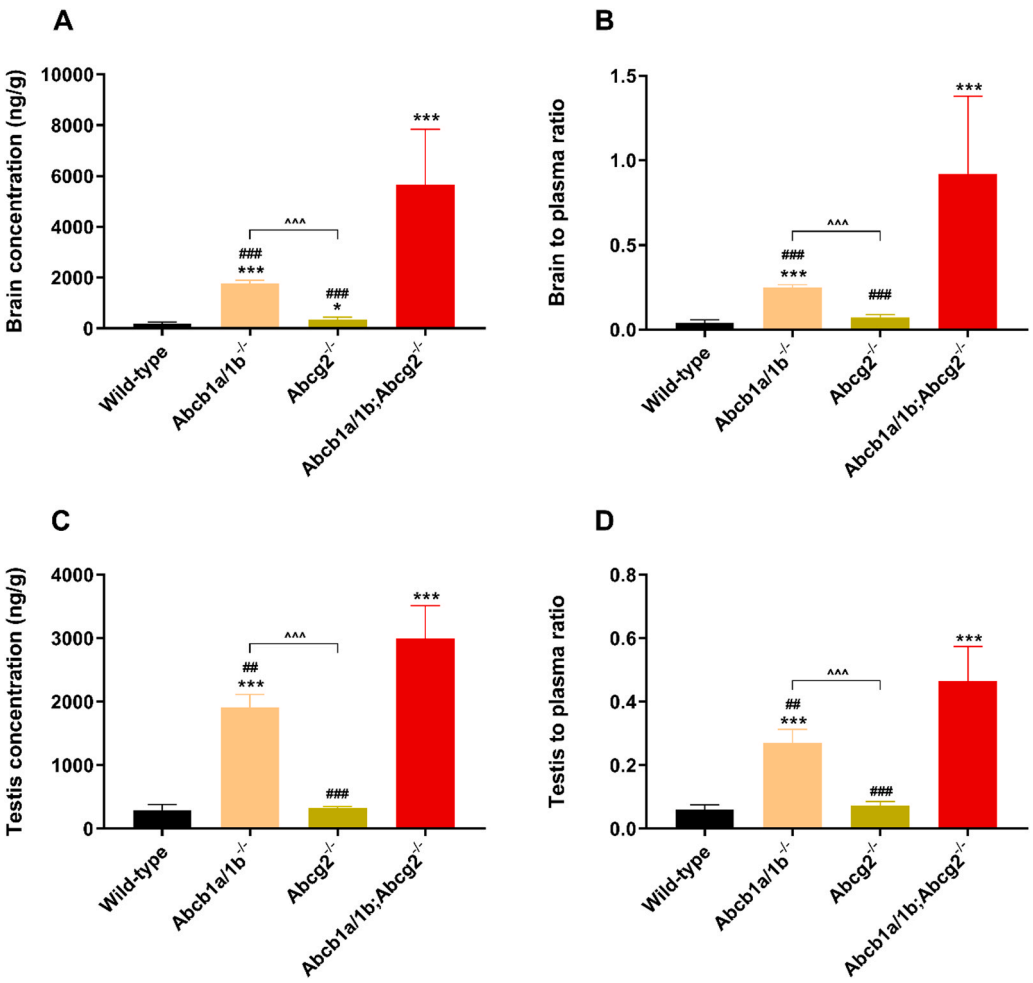

Fig. 3. Brain and testis concentrations (A and C) and tissue-to-plasma ratios (B and D) of pralsetinib in male wild-type, *Abcb1a/1b*$^{-/-}$, *Abcg2*$^{-/-}$ and *Abcb1a/1b;Abcg2*$^{-/-}$ mice over 2 h after oral administration of 10 mg/kg pralsetinib. Data are given as mean ± S.D. (n = 6). * $P < 0.05$; ** $P < 0.01$; *** $P < 0.001$ compared to wild-type mice; # $P < 0.05$; ## $P < 0.01$; ### $P < 0.001$ compared to *Abcb1a/1b;Abcg2*$^{-/-}$ mice. Statistical analysis was applied after log-transformation of linear data.

Cyp3aXAV mice showed a markedly slower relative elimination of pralsetinib than *Cyp3a*$^{-/-}$ mice (Fig. 6B). This unexpected result not only suggests that human CYP3A4 metabolized pralsetinib very little *in vivo*, but also that an alternative pralsetinib elimination mechanism was down-regulated in Cyp3aXAV mice.

Interestingly, the average pralsetinib plasma $AUC_{0-8\,h}$ in wild-type and Cyp3aXAV mice were 30,427 ng/ml * h and 48,865 ng/ml * h (Table 3), respectively, whereas 400 mg pralsetinib once daily in patients yielded a plasma $AUC_{0-24\,h}$ of 43,900 ng/ml * h. The overall pralsetinib plasma exposure in mice in our study and in human patients is therefore quite similar. With respect to the tissue distribution at 8 h, the observed differences in absolute tissue concentrations between the strains in brain, liver, testis, lung, and spleen mostly reflected the differences in plasma concentrations: the tissue-to-plasma ratios were not substantially altered between the strains, perhaps excepting the clearing organs kidney and small intestine (Supplemental Figs. 10 and 11). Collectively, these results suggest that pralsetinib is modestly metabolized by mouse Cyp3a, but not by human CYP3A4. In addition, the elimination of pralsetinib may be in part controlled by an (as yet unidentified) detoxification mechanism other than CYP3A, that is downregulated in Cyp3aXAV mice. This unknown detoxification mechanisms is unlikely to be a hepatic OATP transporter, as the liver-to-plasma ratio was unchanged in the Cyp3aXAV mice (Supplemental Fig. 10), but it might be an apical ABC transporter, given the slightly reduced SI- and SIC-to plasma ratios in these mice (Supplemental Fig. 11). However, these shifts are so modest that downregulation of a pralsetinib-metabolizing enzyme is also a distinct possibility.

4. Discussion and conclusions

This study shows that the RET inhibitor pralsetinib is a transported substrate by ABCB1 and ABCG2 and these transporters affect the *in vivo* bioavailability and distribution of pralsetinib in mice. *In vitro,* pralsetinib was transported very efficiently by human ABCB1 and mouse Abcg2, but not by human ABCG2 and this transport could be completely inhibited by specific small-molecule ABCB1 and ABCG2 inhibitors. The oral availability of pralsetinib was modestly restricted by ABCB1. Moreover, ABCB1 P-gp in the blood-brain-barrier (BBB) could strongly restrict the brain penetration of pralsetinib, while ABCG2 had a more modest effect. Similar functions of ABCB1 and ABCG2 also showed up in the blood-testis-barrier (BTB), albeit somewhat less pronounced. Despite the highly increased brain concentration (30.4-fold), no acute spontaneous pralsetinib toxicity was observed in the *Abcb1a/1b;Abcg2*$^{-/-}$ mice. Of note, at the dose used in our study, the average T_{max} (~2 h), C_{max} (5000–6000 ng/ml) and $AUC_{0-8\,h}$ (30,427 ng/ml * h) of pralsetinib in wild-type mice were of the same order of magnitude as those observed in patients (T_{max} ranging from 2 to 4 h with average C_{max} 2830 ng/ml and $AUC_{0-24\,h}$ 43,900 ng/ml * h) [13].

We also observed a markedly decreased percentage of dose of pralsetinib remaining in the small intestine contents in the absence of Abcb1a/1b, and this decrease was not further enhanced when both Abcb1a/1b and Abcg2 were deficient. This suggests that Abcb1a/1b, but

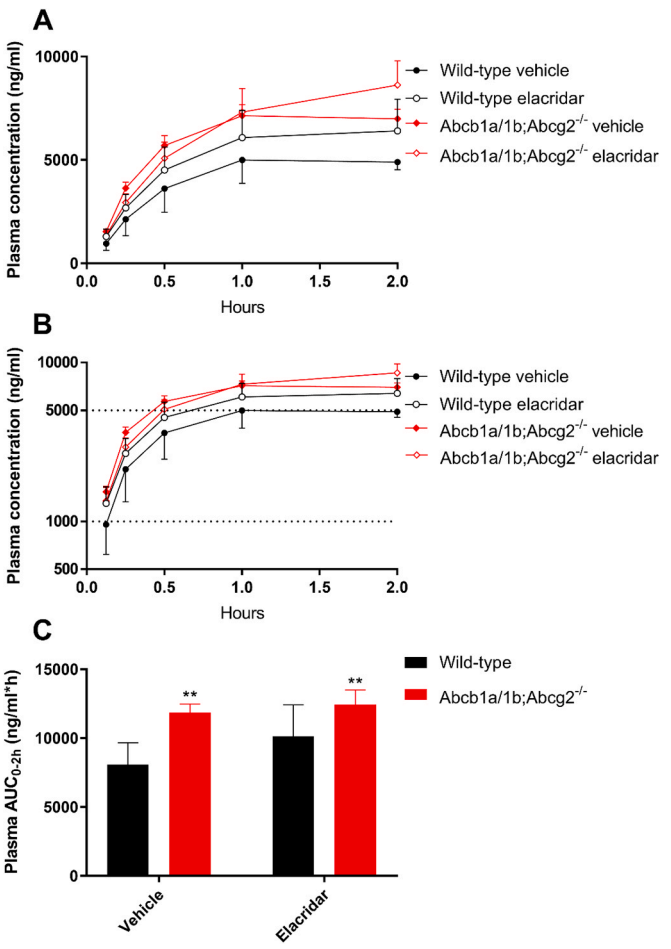

Fig. 4. Plasma concentration-time curves (A), semi-log plot of plasma concentration-time curves (B) and plasma $AUC_{0-2\,h}$ (C) of pralsetinib in male wild-type and *Abcb1a/1b;Abcg2*$^{-/-}$ mice over 2 h after oral administration of 10 mg/kg pralsetinib with or without co-administration of elacridar. Data are given as mean ± S.D. (n = 6). * $P < 0.05$; ** $P < 0.01$; *** $P < 0.001$ compared to wild-type mice. Statistical analysis was applied after log-transformation of linear data.

not Abcg2, can mediate either the direct efflux of pralsetinib across the intestinal wall (also reducing net intestinal uptake) or the hepatobiliary excretion of pralsetinib or a combination of both processes. No substantial changes in tissue distribution due to the ABC transporter deficiencies were found in other tissues including liver, kidney, lung and spleen. OATP1A/1B proteins also did not show a substantial influence on pralsetinib distribution in mice. Taking everything together, our results appear to be generally in line with FDA documentation, in which pralsetinib is mentioned to be a substrate of P-gp and BCRP, but not a substrate of the organic anion transporting polypeptides OATP1B1 and OATP1B3 *in vitro*.

It is striking that the impact of Abcb1a/1b and Abcg2 on the relative brain penetration of pralsetinib (~23-fold reduction) is far higher than on the oral availability of this drug (~1.5-fold reduction). The most likely explanations for this apparent discrepancy are that: 1), the drug concentration in the small intestinal lumen shortly after drug administration is far higher than in the blood that exposes the BBB, making initial saturation of the ABC transporters in the intestine more likely; 2), the overall xenobiotic permeability of the intestinal epithelium, containing countless uptake systems for various nutrients, will likely be much higher than that for the highly selective BBB, which makes it harder for the ABC efflux transporters to effectively counteract a substantial influx of pralsetinib in the intestine; 3), there are likely more alternative drug detoxification systems (*e.g.*, drug-metabolizing systems) in the small intestine and liver for pralsetinib than in the BBB, which makes the relative contribution of the ABC transporters in restricting pralsetinib levels more limited in the small intestine than in the BBB. 4), we further cannot exclude that the membrane density of the ABC transporters in the BBB is higher than in the small intestine, but because of the intestinal microvilli it is hard to give exact numbers on such parameters.

RET fusions occur in lung cancers with a frequency of 1–2%. In 2018, Drilon et al. [42] focused on the frequency, responsiveness, and overall outcomes in RET-rearranged advanced NSCLC patients with central nervous system (CNS) metastases. They showed that the frequency of CNS involvement in these patients is 25% at diagnosis, but lifetime prevalence can reach almost 50%. Furthermore, the cumulative incidence of CNS lesions in RET-positive NSCLC patients is higher than in ROS1-positive but lower than in ALK-positive patients. They also found a low intracranial response rate when these patients were treated with various multikinase inhibitors. However, these outcomes could be due to the limited efficacy of multikinase inhibitors in RET-rearranged NSCLC patients. Whereas for pralsetinib, according to the clinical phase 1/2 trial results and the FDA document [13], responses in intracranial lesions were observed in 4 out of 8 patients including 2 patients with a CNS complete response in metastatic RET fusion-positive NSCLC previously treated with platinum chemotherapy patients. Based on our data, brain penetration of pralsetinib was actually quite low in wild-type mice and this low penetration could be enhanced by up to 32.3-fold due to both ABCB1 and ABCG2 deficiency or inhibition. This brain accumulation enhancement might perhaps further benefit treatment of the NSCLC brain metastasis patients. As also tumors that themselves express significant levels of ABCB1 and/or ABCG2 might become relatively drug resistant, there could be an added benefit to such an inhibitor approach [19,43].

Therefore, in order to further investigate the potential benefit of ABC efflux transporter inhibition, aiming to obtain higher drug efficacy, especially in brain, we tested a potentially clinically realistic schedule to largely or completely inhibit both ABCB1a/1b and ABCG2 in the BBB by co-administration of the pharmacological inhibitor elacridar. Pretreatment with elacridar increased oral availability of pralsetinib in wild-type mice. Moreover, brain distribution of pralsetinib was profoundly improved in wild-type mice by elacridar (from 0.026 to 0.51, 19.6-fold), albeit not to as high a level as seen in vehicle-treated *Abcb1a/1b;Abcg2*$^{-/-}$ mice (0.83, 31.9-fold). Unexpectedly, brain distribution of pralsetinib in *Abcb1a/1b;Abcg2*$^{-/-}$ mice with elacridar was lower than that in *Abcb1a/1b;Abcg2*$^{-/-}$ mice without elacridar, suggesting that some other pralsetinib transport system (perhaps mediating pralsetinib brain uptake) might be affected by elacridar. Our findings on elacridar efficacy could provide a rationale for enhanced treatment of brain metastasis of NSCLC patients by boosting brain penetration of pralsetinib using co-administration of an efficacious ABCB1/ABCG2 inhibitor. Of note, we previously observed severe CNS toxicity in a brigatinib pharmacokinetic study in *Abcb1a/1b;Abcg2*$^{-/-}$ or elacridar-treated wild-type mice [44]. Although there was no acute toxicity observed in mice in the current study, any attempts to enhance pralsetinib overall exposure or brain accumulation in patients using ABCB1/ABCG2 inhibitors should first be carefully monitored for safety.

We further found that pralsetinib oral availability in mice was somewhat restricted by mouse Cyp3a (1.4-fold), but this increased plasma exposure was not rescued by human CYP3A4 expressed in *Cyp3a*-deficient mice. We did not observe any meaningful changes in tissue-to-plasma ratios, suggesting that the differences in tissue concentrations simply reflected the different plasma concentrations among the three mouse strains. These results suggest that CYP3A, and especially human CYP3A4, may not play a substantial role in the metabolic clearance of pralsetinib. It is worth noting that our results seem partly in contradiction with the FDA data, which indicate that pralsetinib is primarily metabolized by CYP3A4 and to a lesser extent by CYP2D6 and

Table 2
Plasma and organ pharmacokinetic parameters of pralsetinib in male wild-type and *Abcb1a/1b;Abcg2*$^{-/-}$ mice over 2 h after oral administration of 10 mg/kg pralsetinib with or without inhibitor elacridar.

Parameter	Genotype/Groups			
	Vehicle		Elacridar	
	Wild-type	*Abcb1a/1b;Abcg2*$^{-/-}$	Wild-type	*Abcb1a/1b;Abcg2*$^{-/-}$
$AUC_{0-2\,h}$, ng/ml*h	8067 ± 1605	11,860 ± 608**	10,119 ± 2299	12,416 ± 1074**
Fold change $AUC_{0-2\,h}$	1.0	1.5	1.3	1.5
C_{max}, ng/ml	5297 ± 816	7360 ± 256**	6432 ± 1519	8845 ± 773***##
T_{max}, h	1.5 ± 0.55	1.3 ± 0.5	1.8 ± 0.41	1.8 ± 0.41
C_{brain}, ng/g	126 ± 20	5778 ± 722***###	3300 ± 1136***	4474 ± 517***#
Fold increase C_{brain}	1.0	45.9	26.2	35.5
Brain-to-plasma ratio	0.026 ± 0.0038	0.83 ± 0.086***###	0.51 ± 0.075***	0.52 ± 0.063***^^^
Fold increase ratio	1.0	31.9	19.6	20.0
C_{Liver}, ng/g	19,030 ± 1412	23,756 ± 3170*	21,837 ± 4105	25,303 ± 1378**
Fold increase C_{liver}	1.0	1.2	1.1	1.3
Liver-to-plasma ratio	3.9 ± 0.13	3.4 ± 0.30	3.5 ± 0.29	3.0 ± 0.49***
Fold change ratio	1.0	0.87	0.90	0.77
SI + SIC percentage of dose, %	20.2 ± 2.2	7.5 ± 2.7***	8.4 ± 1.8***	11.7 ± 1.3***^^
Fold change ratio	1.0	0.37	0.42	0.58
C_{testis}, ng/g	348 ± 245	3011 ± 590***	2511 ± 553***	3402 ± 559***
Fold increase C_{testis}	1.0	8.7	7.2	9.8
Testis-to-plasma ratio	0.069 ± 0.041	0.43 ± 0.083***	0.39 ± 0.023***	0.40 ± 0.059***
Fold change ratio	1.0	6.2	5.7	5.8

Data are given as mean ± S.D. (n = 6). $AUC_{0-2\,h}$, area under the plasma concentration-time curve; C_{max}, maximum concentration in plasma; T_{max}, time point (h) of maximum plasma concentration; C_{brain}, brain concentration; C_{liver}, liver concentration; SI, small intestine (tissue); SIC, small intestine contents; C_{testis}, testis concentration; * $P < 0.05$; ** $P < 0.01$; *** $P < 0.001$ compared to vehicle treated wild-type mice; # $P < 0.05$; ## $P < 0.01$; ### $P < 0.001$ compared to elacridar treated wild-type mice; ^ $P < 0.05$; ^^ $P < 0.01$; ^^^ $P < 0.001$ compared between vehicle-treated *Abcb1a/1b;Abcg2*$^{-/-}$ and elacridar-treated *Abcb1a/1b;Abcg2*$^{-/-}$ mice. Statistical analysis was applied after log-transformation of linear data.

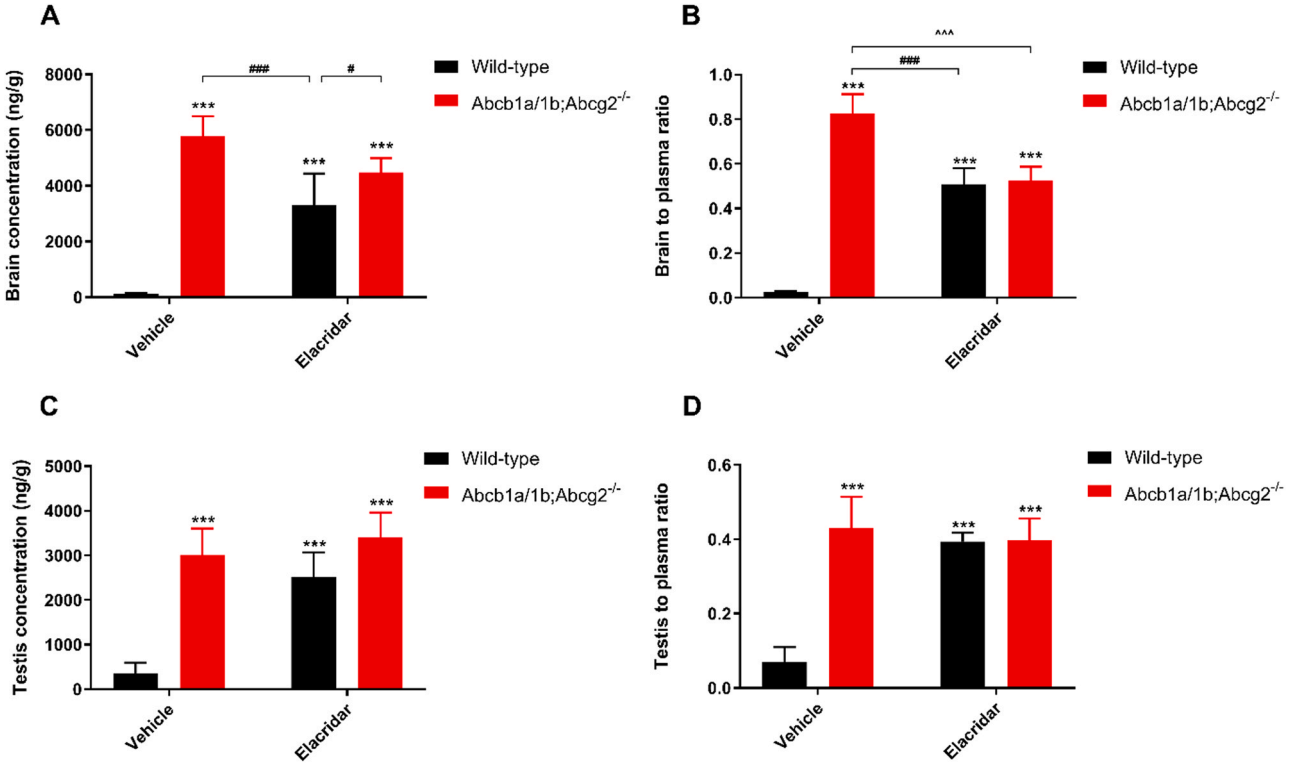

Fig. 5. Brain and testis concentrations (A and C) and tissue-to-plasma ratios (B and D) of pralsetinib in male wild-type and *Abcb1a/1b;Abcg2*$^{-/-}$ mice over 2 h after oral administration of 10 mg/kg pralsetinib with or without co-administration of elacridar. Data are given as mean ± S.D. (n = 6). * $P < 0.05$; ** $P < 0.01$; *** $P < 0.001$ compared to wild-type mice; # $P < 0.05$; ## $P < 0.01$; ### $P < 0.001$ compared to elacridar-treated wild-type mice; ^ $P < 0.05$; ^^ $P < 0.01$; ^^^ $P < 0.001$ compared between vehicle-treated *Abcb1a/1b;Abcg2*$^{-/-}$ and elacridar-treated *Abcb1a/1b;Abcg2*$^{-/-}$ mice. Statistical analysis was applied after log-transformation of linear data.

CYP1A2, *in vitro*. However, our results suggest that there may be one or more other, as yet unidentified, pralsetinib detoxification (elimination) systems downregulated when CYP3A4 is reintroduced, which is/are responsible for the modest pharmacokinetic changes that we observed among the strains. We have previously observed similar compensatory phenomena for the metabolism of midazolam by Cyp3a in Cyp3a

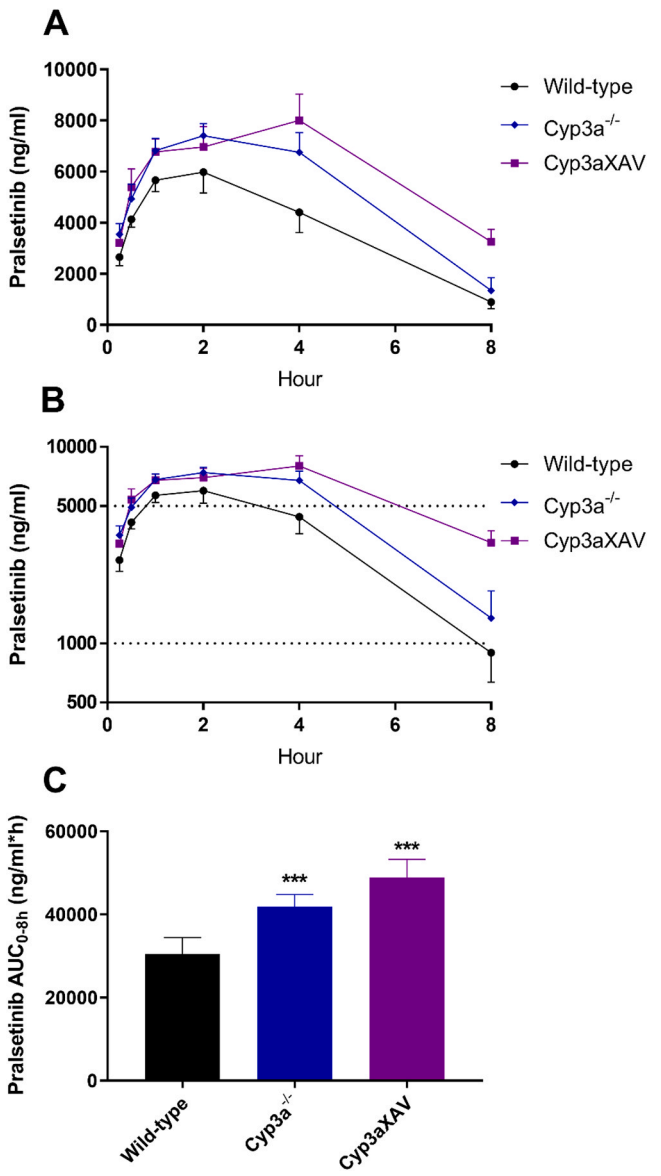

Fig. 6. Plasma concentration-time curves (A), semi-log plot of plasma concentration-time curves (B) and plasma $AUC_{0-8\ h}$ (C) of pralsetinib in female wild-type, *Cyp3a*$^{-/-}$ and Cyp3aXAV mice 8 h after oral administration of 10 mg/kg pralsetinib. Data are given as mean ± S.D. (n = 6). * $P < 0.05$; ** $P < 0.01$; *** $P < 0.001$ compared to wild-type mice; # $P < 0.05$; ## $P < 0.01$; ### $P < 0.001$ compared between *Cyp3a*$^{-/-}$ and Cyp3aXAV mice. Statistical analysis was applied after log-transformation of linear data.

knockout mice [45,46]. Nonetheless, the most likely interpretation of our data is that CYP3A4 itself is not an important determinant of pralsetinib pharmacokinetics in mice.

However, according to FDA guidelines, when pralsetinib (200 mg, QD) was co-administered with the strong CYP3A inhibitor itraconazole (200 mg, QD) in patients, this increased the pralsetinib C_{max} by 84% and $AUC_{0\text{-}INF}$ by 251%. Conversely, co-administration of the CYP3A inducer rifampin (600 mg, QD) with pralsetinib (400 mg, QD) decreased the pralsetinib C_{max} by 30% and the $AUC_{0\text{-}INF}$ by 68% in the clinic. Both findings would be consistent with a significant role for CYP3A in clearing pralsetinib in humans. However, we'd like to emphasize that itraconazole can not only inhibit CYP3A, but also ABCB1. Studies have shown that many of the clinical drug interactions that occur between itraconazole and other drugs are caused by the inhibition of ABCB1 P-gp activity, as well as by the inhibition of CYP3A-mediated metabolism

Table 3
Plasma and organ pharmacokinetic parameters of pralsetinib in female wild-type, *Cyp3a*$^{-/-}$ and Cyp3aXAV mice over 8 h after oral administration of 10 mg/kg pralsetinib.

Parameter	Genotype		
	Wild-type	*Cyp3a*$^{-/-}$	Cyp3aXAV
$AUC_{0-8\ h}$, ng/ml*h	30,427 ± 3975	41,904 ± 2860***	48,865 ± 4339***#
Fold change $AUC_{0-8\ h}$	1.0	1.4	1.6
C_{max}, ng/ml	6067 ± 721	7525 ± 517**	8210 ± 816***
T_{max}, h	1.8 ± 0.41	2.0 ± 1.10	3.7 ± 0.82*#
C_{brain}, ng/g	26.5 ± 10.0	41.5 ± 11.5*	95.6 ± 16.9***###
Fold change C_{brain}	1.0	1.6	3.6
Brain-to-plasma ratio	0.030 ± 0.0058	0.032 ± 0.0054	0.030 ± 0.0055
Fold change ratio	1.0	1.1	1.0
C_{Liver}, ng/g	2796 ± 947	3889 ± 1152	9111 ± 1103***###
Fold change C_{liver}	1.0	1.4	3.3
Liver-to-plasma ratio	3.1 ± 0.28	3.0 ± 0.27	2.8 ± 0.48
Fold change ratio	1.0	0.97	0.90
C_{SI}, ng/g	4286 ± 686	6142 ± 1791*	10,244 ± 1798***##
Fold change C_{SI}	1.0	1.4	2.4
SI-to-plasma ratio	5.0 ± 0.91	4.8 ± 1.0	3.1 ± 0.22***##
Fold change ratio	1.0	0.96	0.62
SIC percentage of dose	3.1 ± 1.3	6.0 ± 1.3**	8.7 ± 2.6***
Fold change %	1.0	1.9	2.8

Data are given as mean ± S.D. (n = 6). $AUC_{0-8\ h}$, area under plasma concentration-time curve; C_{max}, maximum concentration in plasma; T_{max}, time point (h) of maximum plasma concentration; C_{brain}, brain concentration. C_{liver}, liver concentration; SI, small intestine (tissue); C_{SI}, small intestine tissue concentration; SIC, small intestine contents; C_{SIC}, small intestine contents concentration; * $P < 0.05$; ** $P < 0.01$; *** $P < 0.001$ compared to wild-type mice; # $P < 0.05$; ## $P < 0.01$; ### $P < 0.001$ compared between *Cyp3a*$^{-/-}$ and Cyp3aXAV mice. Statistical analysis was applied after log-transformation of linear data.

[47–49]. Moreover, rifampin is also not a completely specific CYP3A inducer. It has been shown that rifampin could also induce many other CYP enzyme family members, as well as some drug transporter proteins, such as intestinal and hepatic P-gp [50,51]. As mentioned above, other pralsetinib detoxification systems may exist and considering that pralsetinib is a good substrate of ABCB1, there is a chance that the increased pralsetinib exposure by itraconazole is due to the inhibition of ABCB1. Furthermore, the decreased pralsetinib exposure by rifampin might be due to the induced function of other CYP enzymes and/or ABCB1 in the FDA drug-drug interaction studies.

In summary, ABCG2 and especially ABCB1, but not OATP1A/1B, can limit the oral availability and brain penetration of pralsetinib. Furthermore, elacridar co-administration could markedly enhance the brain accumulation of oral pralsetinib. Additionally, CYP3A may not be the primary factor responsible for pralsetinib metabolism and elimination *in vivo*, and some other detoxification systems may mediate the elimination of pralsetinib instead. The obtained insights and principles may potentially be used to further enhance the therapeutic application and efficacy of pralsetinib, especially for treatment of brain metastases in NSCLC patients.

CRediT authorship Contribution statement

Yaogeng Wang: Conceptualization, Investigation, Formal analysis, Writing – original draft, Visualization. **Rolf W. Sparidans:**

Methodology, Investigation, Supervision, Writing – review & editing. **Sander Potters:** Investigation, Formal analysis, Writing – review & editing. **Maria C. Lebre:** Resources, Writing – review & editing. **Jos H. Beijnen:** Supervision, Writing – review & editing. **Alfred H. Schinkel:** Term, Conceptualization, Supervision, Writing – original draft, Writing – review & editing, Project administration.

Acknowledgments

This work was funded in part by the Chinese Scholarship Council (CSC Scholarship No. 201506240107 to Y.W.). We gratefully acknowledge Rahime Şentürk for the development and validation of the bioanalytical LC-MS/MS assay at the Utrecht University.

Author contributions

Yaogeng Wang and Alfred H. Schinkel designed the study, analyzed the data and wrote the manuscript. Alfred H. Schinkel administered and supervised the project. Yaogeng Wang, Rolf W. Sparidans, and Sander Potters performed the experimental parts of the study. Maria C. Lebre contributed reagents, materials, and mice. Jos H. Beijnen and Rolf W. Sparidans supervised the bioanalytical part of the studies and checked the content and language of manuscript. All authors commented on and approved the manuscript for submission.

Declaration of interest

The research group of Alfred Schinkel receives revenue from commercial distribution of some of the mouse strains used in this study. The graphical abstract was created with Biorender.com. The remaining authors declare no conflict of interest.

Appendix A. Supporting information

Supplementary data associated with this article can be found in the online version at doi:10.1016/j.phrs.2021.105850.

References

[1] S. Manié, M. Santoro, A. Fusco, M. Billaud, The RET receptor: function in development and dysfunction in congenital malformation, Trends Genet.: TIG 17 (10) (2001) 580–589, https://doi.org/10.1016/s0168-9525(01)02420-9.

[2] E. Arighi, M.G. Borrello, H. Sariola, RET tyrosine kinase signaling in development and cancer, Cytokine Growth Factor Rev. 16 (4–5) (2005) 441–467, https://doi.org/10.1016/j.cytogfr.2005.05.010.

[3] C.F. Ibanez, Structure and physiology of the RET receptor tyrosine kinase, Cold Spring Harb. Perspect. Biol. 5 (2) (2013), https://doi.org/10.1101/cshperspect.a009134.

[4] J.H. Ji, Y.L. Oh, M. Hong, J.W. Yun, H.W. Lee, D. Kim, Y. Ji, D.H. Kim, W.Y. Park, H.T. Shin, K.M. Kim, M.J. Ahn, K. Park, J.M. Sun, Identification of driving ALK fusion genes and genomic landscape of medullary thyroid cancer, PLoS Genet. 11 (8) (2015), 1005467, https://doi.org/10.1371/journal.pgen.1005467.

[5] N. Stransky, E. Cerami, S. Schalm, J.L. Kim, C. Lengauer, The landscape of kinase fusions in cancer, Nat. Commun. 5 (2014) 4846, https://doi.org/10.1038/ncomms5846.

[6] S. Kato, V. Subbiah, E. Marchlik, S.K. Elkin, J.L. Carter, R. Kurzrock, RET aberrations in diverse cancers: next-generation sequencing of 4,871 patients, Clin. Cancer Res.: Off. J. Am. Assoc. Cancer Res. 23 (8) (2017) 1988–1997, https://doi.org/10.1158/1078-0432.Ccr-16-1679.

[7] A. Drilon, Z.I. Hu, G.G.Y. Lai, D.S.W. Tan, Targeting RET-driven cancers: lessons from evolving preclinical and clinical landscapes, Nat. Rev. Clin. Oncol. 15 (3) (2018) 151–167, https://doi.org/10.1038/nrclinonc.2017.175.

[8] R. Elisei, M.J. Schlumberger, S.P. Muller, P. Schoffski, M.S. Brose, M.H. Shah, L. Licitra, B. Jarzab, V. Medvedev, M.C. Kreissl, B. Niederle, E.E. Cohen, L.J. Wirth, H. Ali, C. Hessel, Y. Yaron, D. Ball, B. Nelkin, S.I. Sherman, Cabozantinib in progressive medullary thyroid cancer, J. Clin. Oncol.: Off. J. Am. Soc. Clin. Oncol. 31 (29) (2013) 3639–3646, https://doi.org/10.1200/jco.2012.48.4659.

[9] A. Drilon, N. Rekhtman, M. Arcila, L. Wang, A. Ni, M. Albano, M. Van Voorthuysen, R. Somwar, R.S. Smith, J. Montecalvo, A. Plodkowski, M.S. Ginsberg, G.J. Riely, C. M. Rudin, M. Ladanyi, M.G. Kris, Cabozantinib in patients with advanced RET-rearranged non-small-cell lung cancer: an open-label, single-centre, phase 2, single-arm trial, Lancet Oncol. 17 (12) (2016) 1653–1660, https://doi.org/10.1016/s1470-2045(16)30562-9.

[10] S.A. Wells Jr., B.G. Robinson, R.F. Gagel, H. Dralle, J.A. Fagin, M. Santoro, E. Baudin, R. Elisei, B. Jarzab, J.R. Vasselli, J. Read, P. Langmuir, A.J. Ryan, M. J. Schlumberger, Vandetanib in patients with locally advanced or metastatic medullary thyroid cancer: a randomized, double-blind phase III trial, J. Clin. Oncol.: Off. J. Am. Soc. Clin. Oncol. 30 (2) (2012) 134–141, https://doi.org/10.1200/jco.2011.35.5040.

[11] K. Yoh, T. Seto, M. Satouchi, M. Nishio, N. Yamamoto, H. Murakami, N. Nogami, S. Matsumoto, T. Kohno, K. Tsuta, K. Tsuchihara, G. Ishii, S. Nomura, A. Sato, A. Ohtsu, Y. Ohe, K. Goto, Vandetanib in patients with previously treated RET-rearranged advanced non-small-cell lung cancer (LURET): an open-label, multicentre phase 2 trial, Lancet Respir. Med. 5 (1) (2017) 42–50, https://doi.org/10.1016/s2213-2600(16)30322-8.

[12] Food and Drug Administration, Center for Drug Evaluation and Research of the US Department of Health and Human Service, Food and Drug Administration, Multidiscipline Review, 2020. Available from: ⟨https://www.accessdata.fda.gov/drugsatfda_docs/label/2020/213246s000lbl.pdf⟩.

[13] Food and Drug Administration, Center for Drug Evaluation and Research of the US Department of Health and Human Service, Food and Drug Administration, Multidiscipline Review, 2020. Available from: ⟨https://www.accessdata.fda.gov/drugsatfda_docs/label/2020/213721s000lbl.pdf⟩.

[14] Alexander Drilon, Vivek Subbiah, Geoffrey R. Oxnard, Todd M. Bauer, Vamsidhar Velcheti, Nehal J. Lakhani, Benjamin Besse, Keunchil Park, Jyoti D. Patel, Maria E. Cabanillas, Melissa L. Johnson, Karen L. Reckamp, Valentina Boni, Herbert H.F. Loong, Martin Schlumberger, Ben Solomon, Scott Cruickshank, S. Michael Rothenberg, A.L.J.W. Manisha H. Shah, A phase 1 study of LOXO-292, a potent and highly selective RET inhibitor, in patients with RET-altered cancers, ASCO, 2018, doi: 10.1200/jco.2018.36.15_suppl.102.

[15] V. Subbiah, J.F. Gainor, R. Rahal, J.D. Brubaker, J.L. Kim, M. Maynard, W. Hu, Q. Cao, M.P. Sheets, D. Wilson, K.J. Wilson, L. DiPietro, P. Fleming, M. Palmer, M. I. Hu, L. Wirth, M.S. Brose, S.I. Ou, M. Taylor, E. Garralda, S. Miller, B. Wolf, C. Lengauer, T. Guzi, E.K. Evans, Precision targeted therapy with BLU-667 for RET-driven cancers, Cancer Discov. 8 (7) (2018) 836–849, https://doi.org/10.1158/2159-8290.Cd-18-0338.

[16] S.K. Nigam, What do drug transporters really do? Nat. Rev. Drug Discov. 14 (1) (2014) 29–44, https://doi.org/10.1038/nrd4461.

[17] F.G.M. Russel, Transporters: importance in drug absorption, Distrib., Remov. (2010) 27–49, https://doi.org/10.1007/978-1-4419-0840-7_2.

[18] K.M. Giacomini, S.-M. Huang, D.J. Tweedie, L.Z. Benet, K.L.R. Brouwer, X. Chu, A. Dahlin, R. Evers, V. Fischer, K.M. Hillgren, K.A. Hoffmaster, T. Ishikawa, D. Keppler, R.B. Kim, C.A. Lee, M. Niemi, J.W. Polli, Y. Sugiyama, P.W. Swaan, J. A. Ware, S.H. Wright, S. Wah Yee, M.J. Zamek-Gliszczynski, L. Zhang, Membrane transporters in drug development, Nat. Rev. Drug Discov. 9 (3) (2010) 215–236, https://doi.org/10.1038/nrd3028.

[19] A.H. Schinkel, J.W. Jonker, Mammalian drug efflux transporters of the ATP binding cassette (ABC) family: an overview, Adv. Drug Deliv. Rev. 55 (1) (2003) 3–29.

[20] S.C. Tang, L.N. Nguyen, R.W. Sparidans, E. Wagenaar, J.H. Beijnen, A.H. Schinkel, Increased oral availability and brain accumulation of the ALK inhibitor crizotinib by coadministration of the P-glycoprotein (ABCB1) and breast cancer resistance protein (ABCG2) inhibitor elacridar, Int. J. Cancer 134 (6) (2014) 1484–1494, https://doi.org/10.1002/ijc.28475.

[21] S.C. Tang, N. de Vries, R.W. Sparidans, E. Wagenaar, J.H. Beijnen, A.H. Schinkel, Impact of P-glycoprotein (ABCB1) and breast cancer resistance protein (ABCG2) gene dosage on plasma pharmacokinetics and brain accumulation of dasatinib, sorafenib, and sunitinib, J. Pharmacol. Exp. Ther. 346 (3) (2013) 486–494, https://doi.org/10.1124/jpet.113.205583.

[22] J.S. Lagas, R.A. van Waterschoot, R.W. Sparidans, E. Wagenaar, J.H. Beijnen, A. H. Schinkel, Breast cancer resistance protein and P-glycoprotein limit sorafenib brain accumulation, Mol. Cancer Ther. 9 (2) (2010) 319–326, https://doi.org/10.1158/1535-7163.Mct-09-0663.

[23] H. Kodaira, H. Kusuhara, J. Ushiki, E. Fuse, Y. Sugiyama, Kinetic analysis of the cooperation of P-glycoprotein (P-gp/Abcb1) and breast cancer resistance protein (Bcrp/Abcg2) in limiting the brain and testis penetration of erlotinib, flavopiridol, and mitoxantrone, J. Pharmacol. Exp. Ther. 333 (3) (2010) 788–796, https://doi.org/10.1124/jpet.109.162321.

[24] B. Hagenbuch, P.J. Meier, Organic anion transporting polypeptides of the OATP/SLC21 family: phylogenetic classification as OATP/ SLCO superfamily, new nomenclature and molecular/functional properties, Pflug. Arch.: Eur. J. Physiol. 447 (5) (2004) 653–665, https://doi.org/10.1007/s00424-003-1168-y.

[25] E. van de Steeg, A. van Esch, E. Wagenaar, K.E. Kenworthy, A.H. Schinkel, Influence of human OATP1B1, OATP1B3, and OATP1A2 on the pharmacokinetics of methotrexate and paclitaxel in humanized transgenic mice, Clin. Cancer Res.: Off. J. Am. Assoc. Cancer Res. 19 (4) (2013) 821–832, https://doi.org/10.1158/1078-0432.Ccr-12-2080.

[26] E. van de Steeg, V. Stranecky, H. Hartmannova, L. Noskova, M. Hrebicek, E. Wagenaar, A. van Esch, D.R. de Waart, R.P. Oude Elferink, K.E. Kenworthy, E. Sticova, M. al-Edreesi, A.S. Knisely, S. Kmoch, M. Jirsa, A.H. Schinkel, Complete OATP1B1 and OATP1B3 deficiency causes human Rotor syndrome by interrupting conjugated bilirubin reuptake into the liver, J. Clin. Investig. 122 (2) (2012) 519–528, https://doi.org/10.1172/jci59526.

[27] E. van de Steeg, E. Wagenaar, C.M.M. van der Kruijssen, J.E.C. Burggraaff, D.R. de Waart, R.P. Oude Elferink, K.E. Kenworthy, A.H. Schinkel, Organic anion transporting polypeptide 1a/1b–knockout mice provide insights into hepatic handling of bilirubin, bile acids, and drugs, J. Clin. Investig. 120 (8) (2010) 2942–2952, https://doi.org/10.1172/jci42168.

[28] A. Kalliokoski, M. Niemi, Impact of OATP transporters on pharmacokinetics, Br. J. Pharmacol. 158 (3) (2009) 693–705, https://doi.org/10.1111/j.1476-5381.2009.00430.x.
[29] E. van de Steeg, C.M.M. van der Kruijssen, E. Wagenaar, J.E.C. Burggraaff, E. Mesman, K.E. Kenworthy, A.H. Schinkel, Methotrexate pharmacokinetics in transgenic mice with liver-specific expression of human organic anion-transporting polypeptide 1B1 (SLCO1B1), Drug Metab. Dispos. 37 (2) (2008) 277–281, https://doi.org/10.1124/dmd.108.024315.
[30] A.E. van Herwaarden, E. Wagenaar, C.M. van der Kruijssen, R.A. van Waterschoot, J.W. Smit, J.Y. Song, M.A. van der Valk, O. van Tellingen, J.W. van der Hoorn, H. Rosing, J.H. Beijnen, A.H. Schinkel, Knockout of cytochrome P450 3A yields new mouse models for understanding xenobiotic metabolism, J. Clin. Investig. 117 (11) (2007) 3583–3592, https://doi.org/10.1172/jci33435.
[31] T. Lynch, A. Price, The effect of cytochrome P450 metabolism on drug response, interactions, and adverse effects, Am. Fam. Physician 76 (3) (2007) 391–396.
[32] F.P. Guengerich, Cytochrome P-450 3A4: regulation and role in drug metabolism, Annu. Rev. Pharmacol. Toxicol. 39 (1999) 1–17, https://doi.org/10.1146/annurev.pharmtox.39.1.1.
[33] E. Bakos, R. Evers, G. Calenda, G.E. Tusnady, G. Szakacs, A. Varadi, B. Sarkadi, Characterization of the amino-terminal regions in the human multidrug resistance protein (MRP1), J. Cell Sci. 113 (Pt 24) (2000) 4451–4461.
[34] R. Evers, M. Kool, L. van Deemter, H. Janssen, J. Calafat, L.C. Oomen, C. C. Paulusma, R.P. Oude Elferink, F. Baas, A.H. Schinkel, P. Borst, Drug export activity of the human canalicular multispecific organic anion transporter in polarized kidney MDCK cells expressing cMOAT (MRP2) cDNA, J. Clin. Investig. 101 (7) (1998) 1310–1319, https://doi.org/10.1172/jci119886.
[35] R. Şentürk, Y. Wang, A.H. Schinkel, J.H. Beijnen, R.W. Sparidans, Quantitative bioanalytical assay for the selective RET inhibitors selpercatinib and pralsetinib in mouse plasma and tissue homogenates using liquid chromatography-tandem mass spectrometry, J. Chromatogr. B, Anal. Technol. Biomed. Life Sci. 1147 (2020), 122131, https://doi.org/10.1016/j.jchromb.2020.122131.
[36] Y. Zhang, M. Huo, J. Zhou, S. Xie, PKSolver: an add-in program for pharmacokinetic and pharmacodynamic data analysis in Microsoft Excel, Comput. Methods Prog. Biomed. 99 (3) (2010) 306–314, https://doi.org/10.1016/j.cmpb.2010.01.007.
[37] I. Simoff, M. Karlgren, M. Backlund, A.C. Lindstrom, F.Z. Gaugaz, P. Matsson, P. Artursson, Complete knockout of endogenous Mdr1 (Abcb1) in MDCK cells by CRISPR-Cas9, J. Pharm. Sci. 105 (2) (2016) 1017–1021, https://doi.org/10.1016/s0022-3549(15)00171-9.
[38] J. Wang, M.A.C. Bruin, C. Gan, M.C. Lebre, H. Rosing, J.H. Beijnen, A.H. Schinkel, Brain accumulation of tivozanib is restricted by ABCB1 (P-glycoprotein) and ABCG2 (breast cancer resistance protein) in mice, Int J. Pharm. 581 (2020), 119277, https://doi.org/10.1016/j.ijpharm.2020.119277.
[39] W. Li, M. Tibben, Y. Wang, M.C. Lebre, H. Rosing, J.H. Beijnen, A.H. Schinkel, P-glycoprotein (MDR1/ABCB1) controls brain accumulation and intestinal disposition of the novel TGF-β signaling pathway inhibitor galunisertib, Int. J. Cancer 146 (6) (2020) 1631–1642, https://doi.org/10.1002/ijc.32568.
[40] J. Wang, C. Gan, R.W. Sparidans, E. Wagenaar, S. van Hoppe, J.H. Beijnen, A. H. Schinkel, P-glycoprotein (MDR1/ABCB1) and Breast Cancer Resistance Protein (BCRP/ABCG2) affect brain accumulation and intestinal disposition of encorafenib in mice, Pharmacol. Res. 129 (2018) 414–423, https://doi.org/10.1016/j.phrs.2017.11.006.
[41] Y. Wang, R.W. Sparidans, W. Li, M.C. Lebre, J.H. Beijnen, A.H. Schinkel, OATP1A/1B, CYP3A, ABCB1, and ABCG2 limit oral availability of the NTRK inhibitor larotrectinib, while ABCB1 and ABCG2 also restrict its brain accumulation, Br. J. Pharmacol. 177 (13) (2020) 3060–3074, https://doi.org/10.1111/bph.15034.
[42] A. Drilon, J.J. Lin, T. Filleron, A. Ni, J. Milia, I. Bergagnini, V. Hatzoglou, V. Velcheti, M. Offin, B. Li, D.P. Carbone, B. Besse, T. Mok, M.M. Awad, J. Wolf, D. Owen, D.R. Camidge, G.J. Riely, N. Peled, M.G. Kris, J. Mazieres, J.F. Gainor, O. Gautschi, Frequency of Brain metastases and multikinase inhibitor outcomes in patients with RET-rearranged lung cancers, J. Thorac. Oncol.: Off. Publ. Int. Assoc. Study Lung Cancer 13 (10) (2018) 1595–1601, https://doi.org/10.1016/j.jtho.2018.07.004.
[43] R.W. Robey, K.M. Pluchino, M.D. Hall, A.T. Fojo, S.E. Bates, M.M. Gottesman, Revisiting the role of ABC transporters in multidrug-resistant cancer, Nat. Rev. Cancer 18 (7) (2018) 452–464, https://doi.org/10.1038/s41568-018-0005-8.
[44] W. Li, R.W. Sparidans, Y. Wang, M.C. Lebre, J.H. Beijnen, A.H. Schinkel, P-glycoprotein and breast cancer resistance protein restrict brigatinib brain accumulation and toxicity, and, alongside CYP3A, limit its oral availability, Pharmacol. Res. 137 (2018) 47–55, https://doi.org/10.1016/j.phrs.2018.09.020.
[45] R.A. van Waterschoot, R.W. Rooswinkel, E. Wagenaar, C.M. van der Kruijssen, A. E. van Herwaarden, A.H. Schinkel, Intestinal cytochrome P450 3A plays an important role in the regulation of detoxifying systems in the liver, FASEB J.: Off. Publ. Fed. Am. Soc. Exp. Biol. 23 (1) (2009) 224–231, https://doi.org/10.1096/fj.08-114876.
[46] R.A. van Waterschoot, A.E. van Herwaarden, J.S. Lagas, R.W. Sparidans, E. Wagenaar, C.M. van der Kruijssen, J.A. Goldstein, D.C. Zeldin, J.H. Beijnen, A. H. Schinkel, Midazolam metabolism in cytochrome P450 3A knockout mice can be attributed to up-regulated CYP2C enzymes, Mol. Pharmacol. 73 (3) (2008) 1029–1036, https://doi.org/10.1124/mol.107.043869.
[47] J.J. Lilja, J.T. Backman, J. Laitila, H. Luurila, P.J. Neuvonen, Itraconazole increases but grapefruit juice greatly decreases plasma concentrations of celiprolol, Clin. Pharmacol. Ther. 73 (3) (2003) 192–198, https://doi.org/10.1067/mcp.2003.26.
[48] K.M. Kaukonen, K.T. Olkkola, P.J. Neuvonen, Itraconazole increases plasma concentrations of quinidine, Clin. Pharmacol. Ther. 62 (5) (1997) 510–517, https://doi.org/10.1016/s0009-9236(97)90046-1.
[49] J. Partanen, K.M. Jalava, P.J. Neuvonen, Itraconazole increases serum digoxin concentration, Pharmacol. Toxicol. 79 (5) (1996) 274–276, https://doi.org/10.1111/j.1600-0773.1996.tb00273.x.
[50] J. Chen, K. Raymond, Roles of rifampicin in drug-drug interactions: underlying molecular mechanisms involving the nuclear pregnane X receptor, Ann. Clin. Microbiol Antimicrob. 5 (2006) 3, https://doi.org/10.1186/1476-0711-5-3.
[51] M. Elmeliegy, M. Vourvahis, C. Guo, D.D. Wang, Effect of P-glycoprotein (P-gp) inducers on exposure of P-gp substrates: review of clinical drug-drug interaction studies, Clin. Pharmacokinet. 59 (6) (2020) 699–714, https://doi.org/10.1007/s40262-020-00867-1.